JACS
JOURNAL OF THE AMERICAN CHEMICAL SOCIETY

Article

pubs.acs.org/JACS

Can Contemporary Density Functional Theory Predict Energy Spans in Molecular Catalysis Accurately Enough To Be Applicable for *in Silico* Catalyst Design? A Computational/Experimental Case Study for the Ruthenium-Catalyzed Hydrogenation of Olefins

Kai Rohmann,[†,§] Markus Hölscher,*[,†,§] and Walter Leitner*[,†,‡]

[†]Institut für Technische und Makromolekulare Chemie, RWTH Aachen University, Worringerweg 2, 52074 Aachen, Germany
[‡]Max-Planck-Institut für Kohlenforschung, Kaiser-Wilhelm-Platz 1, 45470 Mülheim a.d. Ruhr, Germany

Supporting Information

ABSTRACT: The catalytic hydrogenation of cyclohexene and 1-methylcyclohexene is investigated experimentally and by means of density functional theory (DFT) computations using novel ruthenium Xantphos^{Ph} (4,5-bis(diphenylphosphino)-9,9-dimethylxanthene) and Xantphos^{Cy} (4,5-bis-(dicyclohexylphosphino)-9,9-dimethylxanthene) precatalysts [Ru(Xantphos^{Ph})($PhCO_2$)(Cl)] (**1**) and [Ru(Xantphos^{Cy})-($PhCO_2$)(Cl)] (**2**), the synthesis, characterization, and crystal structures of which are reported. The intention of this work is to (i) understand the reaction mechanisms on the microscopic level and (ii) compare experimentally observed activation barriers with computed barriers. The Gibbs free activation energy $\Delta G^{\ddagger}$ was obtained experimentally with precatalyst **1** from Eyring plots for the hydrogenation of cyclohexene ($\Delta G^{\ddagger}$ = 17.2 ± 1.0 kcal/mol) and 1-methylcyclohexene ($\Delta G^{\ddagger}$ = 18.8 ± 2.4 kcal/mol), while the Gibbs free activation energy $\Delta G^{\ddagger}$ for the hydrogenation of cyclohexene with precatalyst **2** was determined to be 21.1 ± 2.3 kcal/mol. Plausible activation pathways and catalytic cycles were computed in the gas phase (M06-L/def2-SVP). A variety of popular density functionals (ωB97X-D, LC-ωPBE, CAM-B3LYP, B3LYP, B97-D3BJ, B3LYP-D3, BP86-D3, PBE0-D3, M06-L, MN12-L) were used to reoptimize the turnover determining states in the solvent phase (DF/def2-TZVP; IEF-PCM and/or SMD) to investigate how well the experimentally obtained activation barriers can be reproduced by the calculations. The density functionals B97-D3BJ, MN12-L, M06-L, B3LYP-D3, and CAM-B3LYP reproduce the experimentally observed activation barriers for both olefins very well with very small (0.1 kcal/mol) to moderate (3.0 kcal/mol) mean deviations from the experimental values indicating for the field of hydrogenation catalysis most of these functionals to be useful for *in silico* catalyst design prior to experimental work.

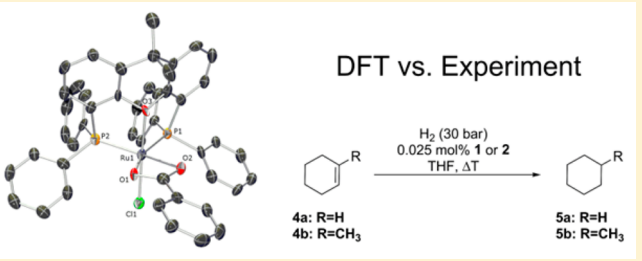

INTRODUCTION

The *in silico* design of the properties (e.g., activity and selectivity) of a molecular catalyst for a desired chemical reaction on the basis of reliable theoretical predictions would be an important step forward to a more rational-based development process in catalysis. Accordingly, the question if such a design of molecular catalysts prior to experimental art is possible on a regular basis is continuously moving further into the focus of theoretical and experimental chemists.[1] The impressive amount of computer resources now available in many academic and industrial research institutions with a tendency of significant future growth has set the technical foundations for an increased use of computer simulations. Another important prerequisite to arrive at such a novel way of designing catalysts and catalytic experiments obviously are theoretical methods which allow for the reliable and accurate prediction of the structures and energies of entire catalytic cycles, including side reactions such as deactivation pathways in acceptable time frames.

Density functional theory (DFT) has made enormous progress in recent years,[2] and the amount of studies which have employed DFT calculations for rationalizing experimental results *post experimentum* is countless. With regard to *a priori* catalyst design the most important question to be addressed is the accuracy of DFT-computed energies. Both catalyst activity and selectivity (e.g., enantio-, regio-, or chemoselectivity) are directly related to the various reaction pathways available to a molecular system. The energy differences between the different pathways can be very small and differ in some cases by only a few tenths of a kilocalory per mole.

Most recent developments showed that modern DFT methods are indeed capable of predicting quantities relevant for catalysis with satisfying accuracy. Such studies have mainly been made possible by the introduction of corrections into the DFT computations which account for dispersion interactions between two (or more) molecules or different parts of the same

Received: November 16, 2015

DOI: 10.1021/jacs.5b11997
J. Am. Chem. Soc. XXXX, XXX, XXX−XXX

molecule. Currently the D-series of corrections (D1−D3) by the Grimme group[3] as well as the so-called Minnesota functionals by the Truhlar group[4] are the most widely used modified recent improvements to DFT, with which the quantitative correlation of computed and experimental results in catalysis and in other fields of chemistry is possible with good accuracy. Studies in which those DFs were used include for instance a variety of investigations referenced to experimental data aiming at the understanding of one or more reaction steps in various chemical transformations closely related to catalysis.[5] A special emphasis was given to the clarification of ligand dissociation energies in ruthenium metathesis catalysts as was described by the groups of Goddard[6] and Truhlar.[7] A focus on barrier heights was given recently in two publications of the Schoenebeck group.[8] A very recent contribution by Gusev focuses on the reaction energies of a quite large variety of reactions taking place at transition metal complexes highlighting the convincing accuracy of the M06-L DF.[9]

Systematic comparisons of experiment and theory in fields strongly relevant for molecular organometallic catalysis and considering full catalytic cycles have appeared only scarcely,[10] especially with regard to the comparison of computed and experimentally derived activation barriers. However, this is an important area, as the development of novel catalysts—especially in *in silico* catalyst design—often is driven by the question if an unknown catalyst will be able to actually perform a desired catalytic reaction. Accordingly, the accurate prediction of the relative energies of the intermediates and transition states of a catalytic cycle is necessary to unequivocally identify the turnover-determining intermediate (TDI) and the turnover-determining transition state (TDTS) as these two stationary points define the energy span (ES),[11] i.e., the effective activation barrier of the reaction. In this study we chose to investigate catalytic olefin hydrogenation as a prototypical reaction of wide application where basic mechanisms are well established to derive plausible catalytic cycles. A novel ruthenium Xantphos-type catalyst system was used for the hydrogenation of olefins with H_2 to arrive at an appreciable comparison of experiment and theory.

We chose complexes **1** and **2** for this study, the synthesis, characterization, and use of which as precatalysts in the catalytic hydrogenation of cyclohexene and 1-methylcyclohexene will be reported here along with an in depth comparison of an experimental and a DFT-computed kinetic analysis. This case study intends to contribute an answer to the question if the experimentally derived ESs are reproduced by DFT with an accuracy high enough to make DFT useful as a predictive tool in catalytic hydrogenations on a regular basis. Beyond energy accuracy also computation times of some DFs are considered. In the final part of the study the DFT computed ES for the hydrogenation of *trans*-stilbene in the presence of **1** as the precatalyst is used to make a prediction about catalyst activity with regard to what can be expected in experiments. Afterward experiments were actually carried out to check the validity of the DFT result showing convincing agreement between experiment and theory.

RESULTS AND DISCUSSION

1. Synthesis and Characterization of 1 and 2. Complexes **1** and **2** were prepared with yields of 78% and 51%, respectively, based on the Ru precursor [{Ru(Cl)$_2$(benzene)$_2$] (**3**) in a two-step synthesis according to a modified literature procedure.[12] In the first step, the respective Xantphos ligand coordinates to the metal center by heating it with **3** in a toluene/ethanol mixture at 100 °C for 90 min. Subsequent addition of sodium benzoate in a slightly substoichiometric amount results in the formation of the corresponding benzoate complexes, which precipitate from the solution if ^{t}BuOH is applied as solvent (Scheme 1).

Scheme 1. Synthesis of 1 and 2

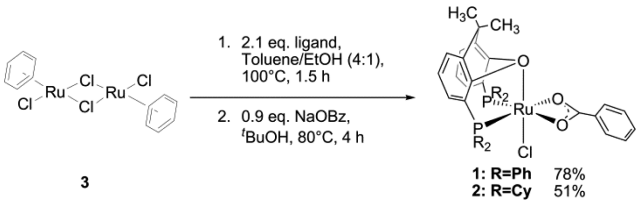

We were able to determine the molecular structure of **1** and **2** by single-crystal X-ray diffraction. Figure 1 shows the structure of complex **1** in the solid state, and a CIF file is provided in the Supporting Information.

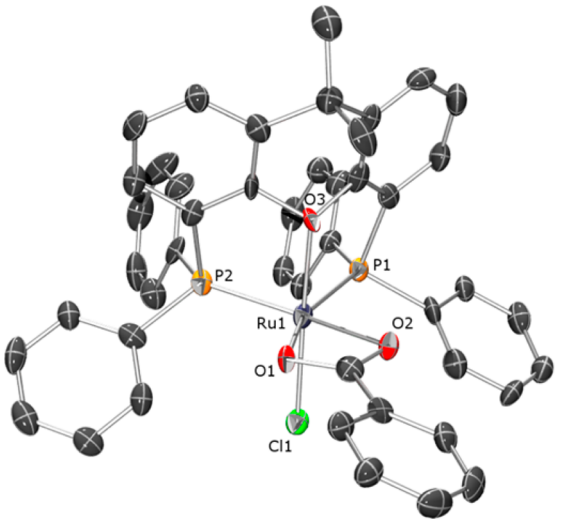

Figure 1. Molecular structure of complex **1** (50% probability level) as obtained from single-crystal X-ray diffraction. Hydrogen atoms are omitted for clarity. Selected bond lengths [Å] and angles [°]: Ru−O1, 2.204; Ru−O2, 2.175; Ru−O3, 2.226; Ru−P1, 2.232; Ru−P2, 2.231; Ru−Cl, 2.371; P1−Ru−P2, 101.84; P1−Ru−O3, 82.96; P2−Ru−O3, 82.89; O1−Ru−O2, 60.42.

The Xantphos^{Ph} ligand coordinates tridentate with the oxygen atom in *trans*-position to the chloro ligand. The distance of the Xantphos oxygen to the ruthenium center is 2.226 Å and thus indicates the κ^3-coordination of the ligand. The benzoate ligand shows a bidentate coordination which completes the octahedral complex geometry. The $^{31}P\{^1H\}$ NMR spectrum of **1** shows a singlet at δ 62.5 ppm, in accord with this structure of the complex also in solution.

The structure of **2** in the crystal shows the ligand to coordinate tridentate as well (Figure 2; a CIF file is provided in the Supporting Information). The Ru−O3 distance clearly indicates the κ^3-coordination of Xantphos^{Cy}. It is with 2.13 Å considerably smaller than the sum of the van der Waals radii for oxygen and ruthenium and is significantly shorter than the Ru−O3 distance of complex **1**. The reason is presumably the higher basicity of the cyclohexyl moieties at the Xantphos ligand. The

DOI: 10.1021/jacs.5b11997
J. Am. Chem. Soc. XXXX, XXX, XXX−XXX

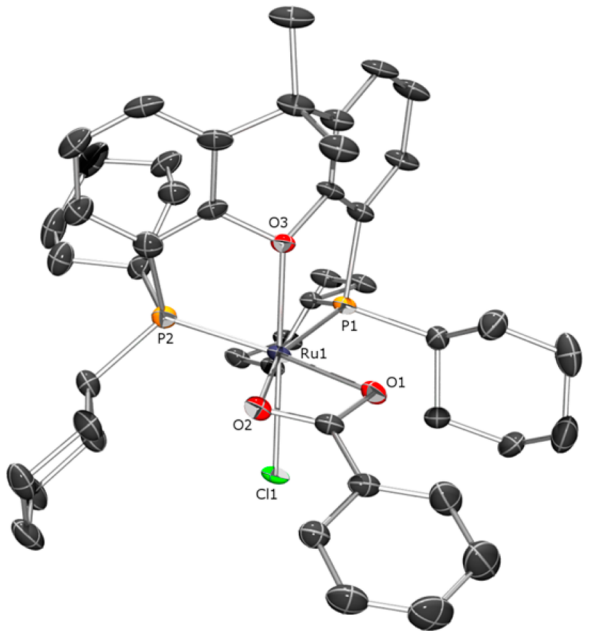

Figure 2. Molecular structure of complex **2** (50% probability level) as obtained from single-crystal X-ray diffraction. Hydrogen atoms are omitted for clarity. Selected bond lengths [Å] and angles [°]: Ru−O1, 2.263; Ru−O2, 2.157; Ru−O3, 2.130; Ru−P1, 2.229; Ru−P2, 2.265; Ru−Cl, 2.355; P1−Ru−P2, 101.87; P1−Ru−O3, 84.04; P2−Ru−O3, 81.47; O1−Ru−O2, 59.48.

chloro ligand is in *trans*-position to the Xantphos oxygen and the benzoate ligand reveals a bidentate coordination, as observed in complex **1** similarly. The $^{31}P\{^{1}H\}$ NMR spectrum of **2** shows a singlet at δ 70.1 ppm, confirming the high symmetry of the complex in solution.

2. Experimental Hydrogenation of Cyclohexene and 1-Methylcyclohexene in the Presence of 1 and 2, Including the Derivation of the Activation Parameters $\Delta H^{\ddagger}$, $\Delta S^{\ddagger}$, and $\Delta G^{\ddagger}$ from Eyring plots. The experimental activation barriers of olefin hydrogenations with **1** and **2** (Scheme 2) were determined from Eyring plots (see Supporting Information (SI) for details). The catalytic hydrogenations showed good reproducibility, and no induction period was observed, revealing that the formation of the active hydrogenation species is fast relative to the catalytic turnover. To obtain the rate constants, we recorded pressure-drop curves for at least four different temperatures and determined the initial reaction rates from the gradient of the curves. The temperatures were chosen in a narrow range, to avoid mass transfer limitations of the reaction at too high reaction rates. Based on a linearized form of the Eyring equation, we calculated the activation parameters from the linear fit of the respective Eyring plot (see SI).

Scheme 2. Hydrogenation of Cyclohexene (4a) and 1-Methylcyclohexene (4b) with Precatalysts 1 and 2

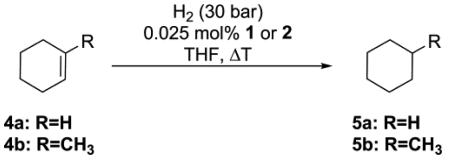

Figure 3 depicts the Eyring plot for the hydrogenation of cyclohexene (**4a**) with **1** as precatalyst in a temperature range between 35 and 50 °C using tetrahydrofuran (THF) as solvent. From the Eyring plot, the Gibbs free activation energy of the reaction was determined to be $\Delta G^{\ddagger}$ = 17.2 ± 1.0 kcal/mol.

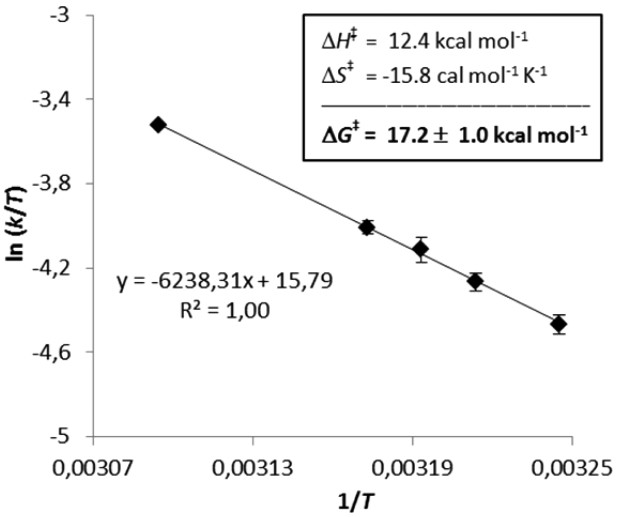

Figure 3. Eyring plot for the hydrogenation of cyclohexene (**4a**) with **1** at five different temperatures (35−50 °C). Average *k* values over at least two runs.

The hydrogenation of 1-methylcyclohexene (**4b**) proceeds with a lower reaction rate. The experimental $\Delta G^{\ddagger}$ of the reaction is 18.8 ± 2.4 kcal/mol (Figure 4). This result is in line with the expectations, because substituted double bonds are less reactive in organometallic hydrogenation.

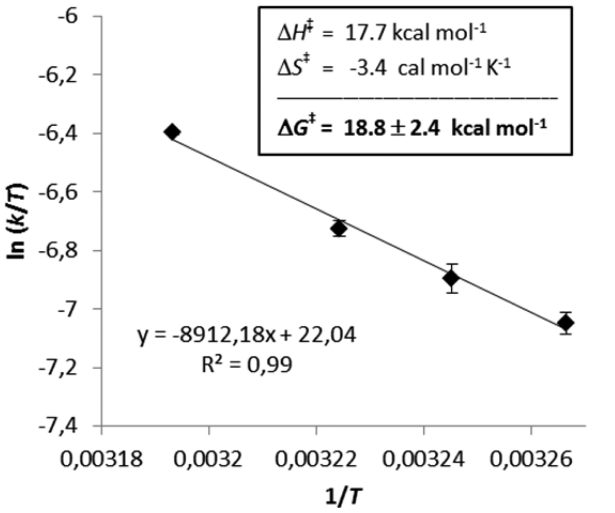

Figure 4. Eyring plot for the hydrogenation of 1-methylcyclohexene (**4b**) with **1** at four different temperatures (33−40 °C). Average *k* values over at least two runs.

To investigate the influence of a change in the ligand structure on the hydrogenation of **4a**, complex **2**, in which the Xantphos ligand bears cyclohexyl moieties at the P-atoms, was applied as precatalyst. The hydrogenation proceeds significantly slower in comparison to the hydrogenation with **1**. The Gibbs free activation barrier $\Delta G^{\ddagger}$ as obtained from the Eyring plot (Figure 5) amounts to 21.1 ± 2.3 kcal/mol.

DOI: 10.1021/jacs.5b11997
J. Am. Chem. Soc. XXXX, XXX, XXX−XXX

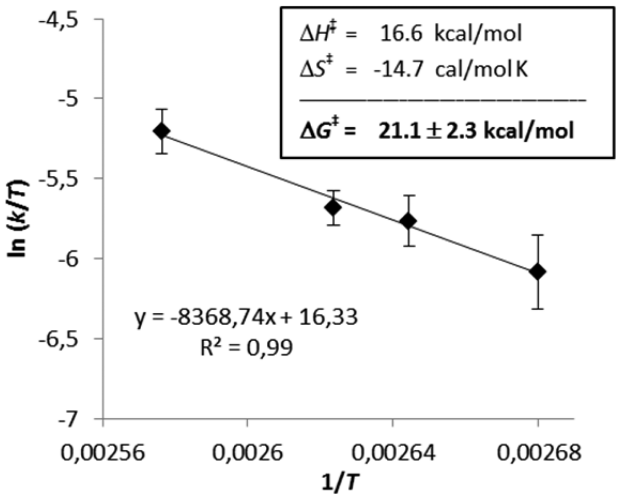

Figure 5. Eyring plot for the hydrogenation of cyclohexene (**4a**) with **2** at four different temperatures (100−115 °C). Average k values over at least two runs.

The Eyring plot for the hydrogenation reaction with precatalyst **2** shows a slightly broader error margin of the single experiments compared to the experiments with precatalyst **1**. This reflects the higher sensitivity of the active species which is formed from **2** toward deactivation by impurities.

3. Development and Computation of Plausible Catalytic Cycles for the Hydrogenation of Cyclohexene and 1-Methylcyclohexene in the Presence of 1 and 2, Including a Thorough Comparison of Various DFs with Experimental Data. To compare the experimentally obtained activation parameters with computational data, a plausible catalytic cycle for the hydrogenation of the olefins **4a** and **4b** with precatalysts **1** and **2** was developed in the next step (Scheme 3). Prior to the catalytic hydrogenation of the corresponding olefin, the active species of the catalyst has to be formed. Since the precatalysts are benzoate complexes, we considered a plausible activation pathway to be the hydrogenolysis of the carboxylate to benzoic acid with concomitant formation of a classical hydride complex (**V_Solvent**) which is the active species. This is supported by the detection of hydrogenation products of benzoic acid in the reaction mixture.

Catalyst Activation. In the first step of the activation pathway, the benzoate ligand has to change its coordination mode from κ^2 to κ^1 (**TSI_II**), and a hydrogen molecule can occupy the free coordination site (**II**). The hydrogen molecule is subsequently cleaved heterolytically (**TSII_III**) leading to a classical hydride complex, with a coordinated molecule of benzoic acid (**III**). This acid molecule flips to build a hydrogen bridge with the chloro ligand (**IV**) and is finally substituted by a solvent molecule (**V_Solvent**). Unless otherwise noted, the coordinating solvent molecule was considered to be THF, because this was used in the experimental hydrogenations as the reaction medium.

Catalytic Cycle. Structure **V_Solvent** is the entry point into the catalytic cycle of the olefin hydrogenation. The coordinated solvent is replaced by a substrate molecule, forming a π-complex (**VI**). Subsequently, the hydrido ligand is transferred to the *cis*-coordinated carbon atom of the olefin (**TSVI_VII**). This step leads to complex **VII**, which has a vacant coordination site and a σ-bonded cyclohexyl ligand. The free coordination site of **VII** is saturated by an agostic interaction with the cyclohexyl ligand until it is occupied by either a solvent molecule (**VII_Solvent**) or a hydrogen molecule (**VIII**). **VII_Solvent** is richer in energy in all cases studied in this work and therefore does not contribute to the ES. The last step of the catalytic cycle is the reaction between the cyclohexyl ligand and the hydrogen molecule (**TSVIII_V**), resulting in a free cyclohexane molecule and coordination of a solvent molecule regenerating the hydrido complex **V_Solvent**.

We studied the proposed reaction pathway for the hydrogenation of olefins by means of DFT calculations (Gaussian09, revision D.01; for details see SI).[13] To identify the key steps of the reaction, which are the highest and lowest points on the energy hypersurface, we calculated the complete gas-phase energy profile on M06-L/def2-SVP(ECP) level (see SI for details) and subsequently reoptimized the characteristic points using the larger def2-TZVP basis set in the gas phase and independently also in combination with a variety of different density functionals with implicit inclusion of solvent effects (see also the SI for referencing the M06-L/def2-TZVP gas-phase energies to DLPNO-CCSD(T)/def2-TZVP energies).

Figure 6 depicts the energy profile for precatalyst **1** in the hydrogenation of cyclohexene (**4a**) to the saturated product **5a**. According to the ES model, the effective activation barrier for a catalytic cycle is determined by the intermediate and the transition state with the highest Gibbs free energy difference, defined previously as the TDI and TDTS, respectively,[11] and the activation barrier is the energy span ES. In this case, the formation of the active species does not contribute to the energy span of the olefin hydrogenation. We were able to show experimentally, that the benzoic acid molecule, which is formed while the catalyst is activated, is hydrogenated to a mixture of benzaldehyde and benzyl alcohol, which excludes that an equilibrium between the catalytic hydrogenation and the formation of the active catalyst exists (see Scheme 3 and SI). Therefore, the ES of the olefin hydrogenation is the energy difference between **VII** being the TDI and **TSVIII_V** being the TDTS. Complex **VII_Solvent** does not affect the ES, since the corresponding minimum is less stable than **VII**. The gas-phase ES for the cyclohexene hydrogenation is 17.0 kcal/mol at the M06-L/def2-SVP(ECP) level.

We reoptimized the key steps of the energy profile, i.e., the TDI (**VII**) and the TDTS (**TSVIII_V**) as well as **V_Solvent**, with different density functionals and implicit solvent correction to determine the influence of different functionals and solvent models on the calculated activation barrier (Figure 7). It turned out that, for a few methods, structure **VII** is the TDI, whereas in most cases, **V_Solvent** is the lowest minimum in the catalytic cycle. The ES was consequently determined as the energy difference between the lowest intermediate in the particular case and the highest transition state, which was always **TSVIII_V**.

When looking at the solvent-phase calculations, it can be seen, that the experimental activation barrier can be reproduced by the Minnesota functional MN12-L with good accuracy (Figure 7). B3LYP overestimates the ES slightly, due to the lack of dispersion corrections, however, not overly so in this particular case. Augmentation of B3LYP with Grimmes D3 dispersion correction (B3LYP-D3), gives a very satisfying result, showing the significance of the dispersion correction for the calculated ES. CAM-B3LYP is as accurate as B3LYP. The drawback of B3LYP and CAM-B3LYP are of course the significantly longer computing times compared to other DFs which yield the same accuracy in much shorter times. The most

DOI: 10.1021/jacs.5b11997
J. Am. Chem. Soc. XXXX, XXX, XXX−XXX

Scheme 3. Proposed Formation of the Active Hydrogenation Species from the Precatalysts (1 or 2) and Catalytic Cycle for the Hydrogenation of Cyclohexene (4a)

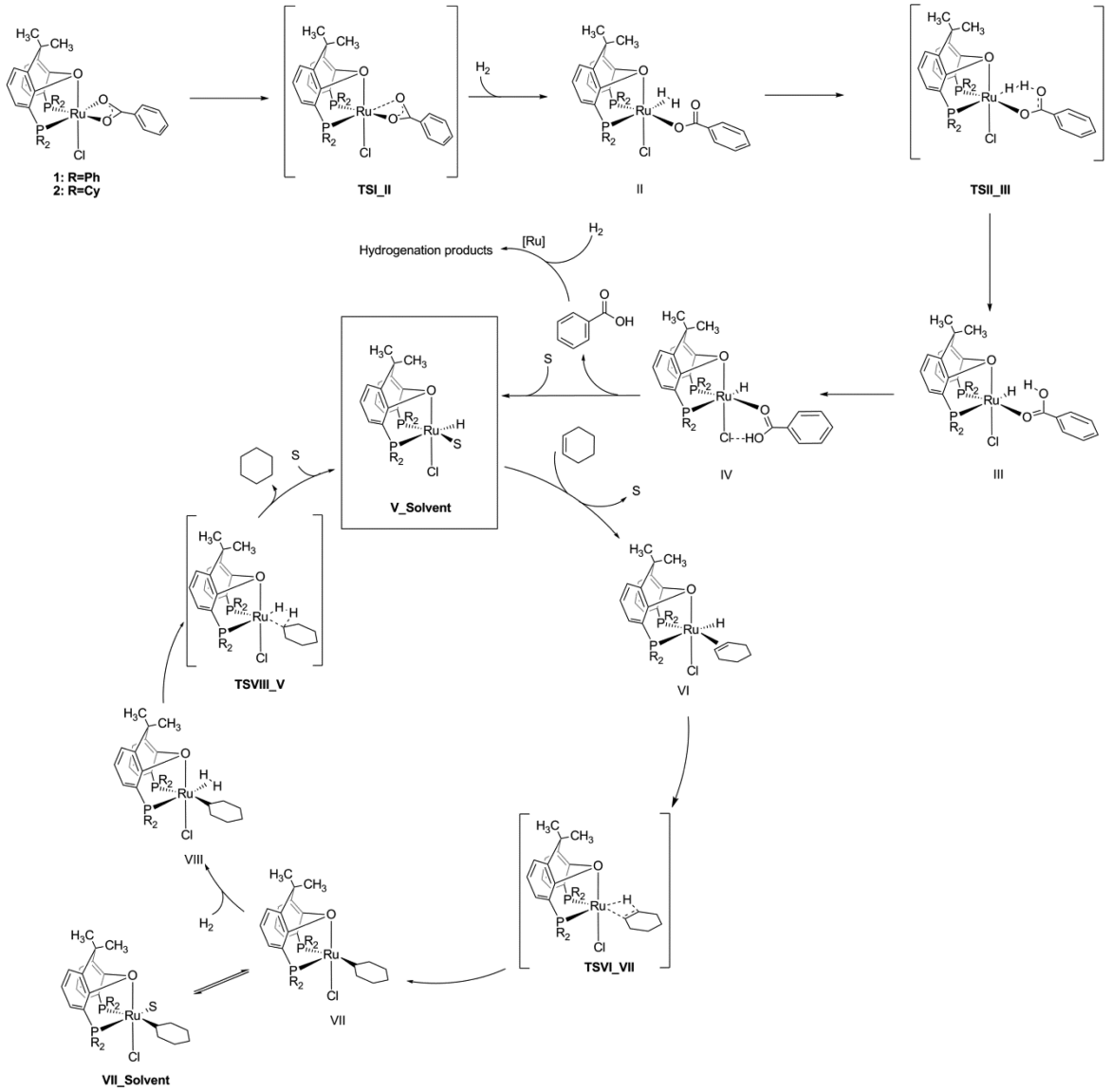

serious deviations between experiment and calculations are observed with ωB97X-D, LC-ωPBE, PBE0-D3, and BP86-D3. All four DFs underestimate the experimental values drastically. The result for BP86 is in agreement with the previously reported poor accuracy in the prediction of activation barriers.[8b] Notable is the accurate performance of B97-D3BJ since it reproduces the experimental $\Delta G^{\ddagger}$ with an accuracy in the range of MN12-L and B3LYP-D3, but the calculations are much faster.

Additionally, we compared the experimental and computational activation enthalpies ($\Delta H^{\ddagger}$) using the above-mentioned DFT methods (Figure 8). The experimentally determined value is 12.4 ± 0.3 kcal/mol. Overall, the accuracy of $\Delta H^{\ddagger}$ for the corresponding functionals is in the same range as for the calculation of the Gibbs free activation enthalpies $\Delta G^{\ddagger}$. MN12-L as well as B97-D3BJ and B3LYP-D3 give good to excellent results. However, the computing time shows significant differences. It is notable, that the functionals with low accuracy in reproducing the experimentally derived $\Delta G^{\ddagger}$ value also show an explicit deviation from the experimental $\Delta H^{\ddagger}$ value. One can therefore conclude, that the low accuracy of ωB97X-D, LC-ωPBE, PBE0-D3, and BP86-D3 is not caused by a deficient calculation of the entropy, but by the calculation of the electronic energy, which seems to be insufficient for reproducing ESs.

We then chose substrate **4b**, in order to analyze if the calculations are able to reproduce the results for this reaction as well and if the correct trend for the activation barrier is predicted. For the hydrogenation of **4b**, the activation of the precatalyst **1** is exactly the same as for **4a**. Thus, minimum **VI** is the first point of the energy profile, where the substrate interacts with the catalyst. However, for the catalytic hydrogenation of **4b**, there are two possible pathways (Figure 9).

In path 1, a hydrido ligand is transferred first to the unsubstituted carbon atom of the double bond whereas in path 2, the hydrido ligand is transferred to the substituted carbon atom in the first instance. Figure 10 depicts the Gibbs free energy profile for both cycles and shows that path 2 is energetically clearly preferred over path 1. All minima and transition states of path 2 are more stable than the

DOI: 10.1021/jacs.5b11997
J. Am. Chem. Soc. XXXX, XXX, XXX−XXX

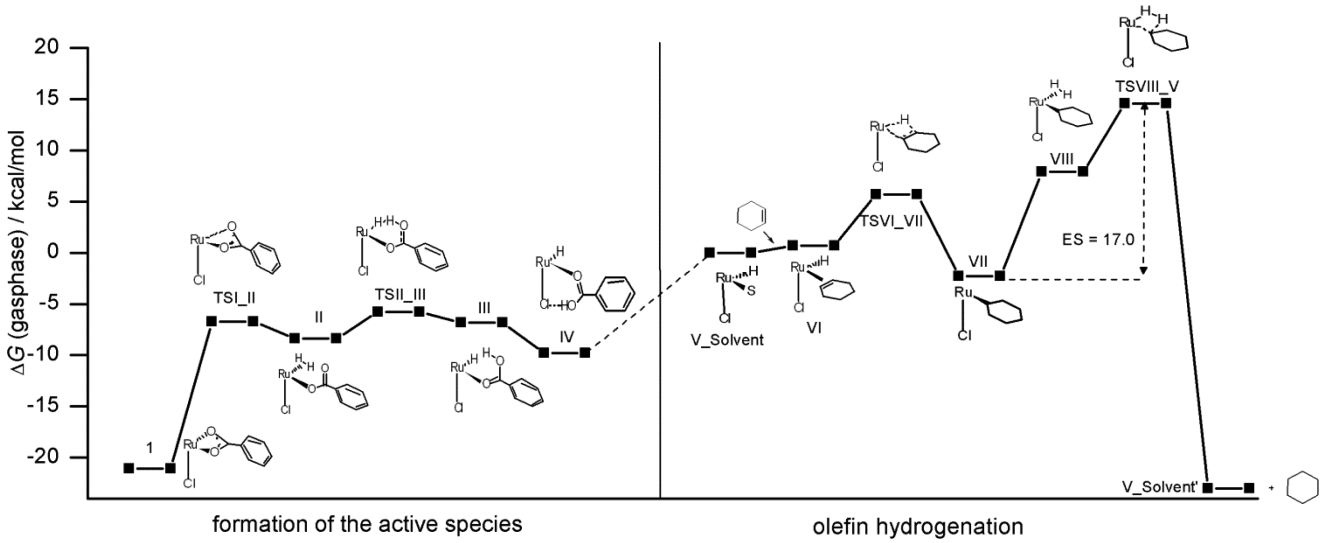

Figure 6. Gibbs free energy profile for the hydrogenation of cyclohexene (**4a**) with precatalyst **1** and energy span (ES).

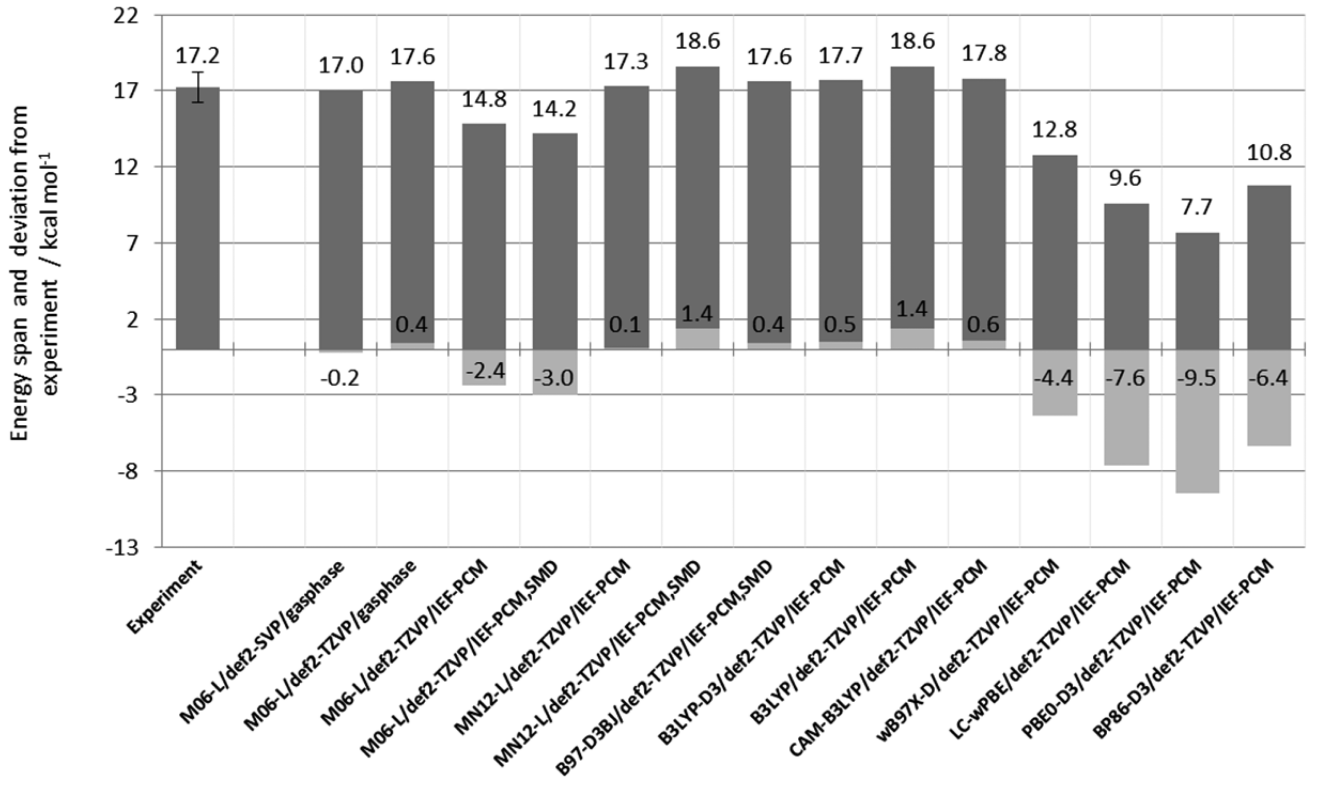

Figure 7. Experimental and computational energy spans (dark gray) and deviations from experiment (light gray) for the hydrogenation of **4a** with **1** as precatalyst. Solvent model calculations were performed with THF as solvent (see SI for details).

corresponding structures in path 1. Hence, the ES for path 2 is lower, with 15.4 kcal/mol compared to 25.8 kcal/mol for path 1. This is a clear indication, that the reaction proceeds via path 2. The ES is thus the energy difference between **V_Solvent** and **TSVIII_V**. As before, the key steps of the profile were calculated with various DFs to see which DFs reproduce the experiment with good accuracy (Figure 11). We took minimum **VII** into account as well, since the energy difference between **V_Solvent** and **VII** is small in this case. However, for all methods **V_Solvent** turned out to be the TDI. Overall, the different DFs yield results similar to the ones obtained for the hydrogenation of **4a** with precatalyst **1**. PBE0-D3 and BP86-D3 underestimate the activation barrier significantly (Figure 11), while the Minnesota functionals are in good (MN12-L) to excellent (M06-L) agreement with the experimentally obtained $\Delta G^{\ddagger}$. B3LYP-D3 is as accurate as the Minnesota functionals, but has the disadvantage of long computing times. B3LYP differs drastically from the dispersion-corrected B3LYP-D3 and overestimates the ES by 6.6 kcal/mol. The difference between B3LYP and the dispersion-corrected B3LYP-D3 shows the importance of the dispersion contribution to the energetics in this case. The best compromise between computing time and accuracy gives again B97-D3BJ, which overestimates the ES by just 1.4 kcal/mol.

DOI: 10.1021/jacs.5b11997
J. Am. Chem. Soc. XXXX, XXX, XXX−XXX

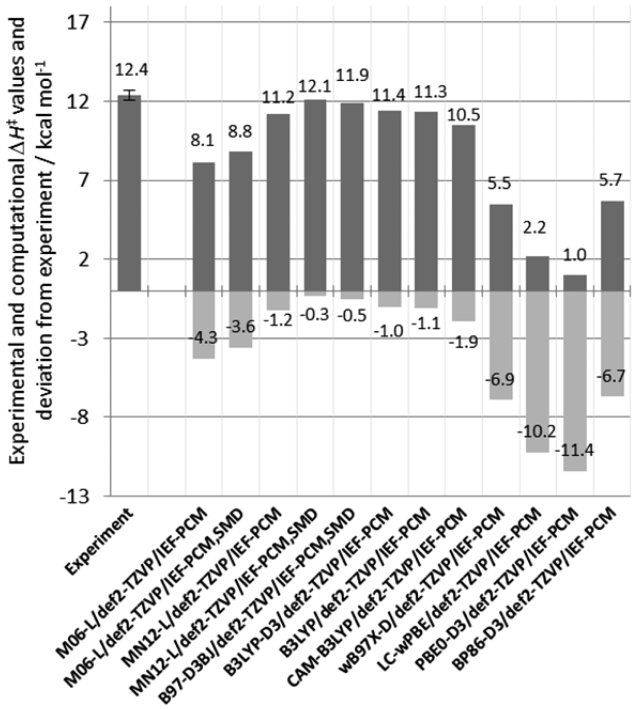

Figure 8. Experimental and computational $\Delta H^{\ddagger}$ values (dark gray) and deviation from experiment (light gray) for the hydrogenation of **4a** with **1** as precatalyst. Solvent model calculations were performed with THF as solvent (see SI for details).

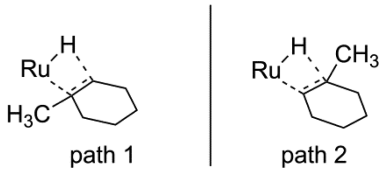

Figure 9. Hydrogenation pathways for substrate **4b**.

All of the methods predict in direct comparison the hydrogenation of **4b** to be slower than the hydrogenation of the unsubstituted olefin **4a**. However, a good agreement of the computed activation barrier with the experimentally derived barrier, which is of high interest for *in silico* catalyst design, is not achieved by PBE0-D3, BP86-D3, and B3LYP.

In the next step we investigated, which of the DFT methods is able to reproduce the experimental activation barrier in case that not the substrate, but the catalyst is modified. Therefore, we calculated the Gibbs free energy profile for the hydrogenation of **4a** with precatalyst **2**, which bears cyclohexyl moieties at the phosphorus atoms. The activation of the catalyst as well as the olefin hydrogenation follow the same mechanism as depicted in Scheme 3. The complete energy profile, which was calculated on M06-L/def2-SVP(ECP) level is shown in Figure 12. For the hydrogenation of olefins with **2**, it is more challenging to find the most stable intermediates and transition states of the energy hypersurface. The reason is, that the cyclohexyl substituents at the phosphines can adopt several conformations compared to phenyl moieties. These various conformations show to some extent a significant difference in energy. It is important to consider these structurally subtle though energetically important changes.[2b,9] Therefore, we optimized a representative set of minima for each point in the energy profile (each minimum and transition state) and chose the lowest energy conformers for constructing the energy profile (details see SI).

The ES is defined by **V_Solvent** and **TSVIII_V**. The coordination of a solvent molecule between steps **VII** and **VIII** does not change the profile, because the resulting solvent complex has a higher energy than **V_Solvent**. The ES on M06-L/def2-SVP(ECP) level is 16.9 kcal/mol. We reoptimized **V_Solvent** and **TSVIII_V** with the previously used DFT methods to analyze which method reproduces the experiment with the highest accuracy (Figure 13).

As for the above-mentioned cases, the Minnesota functionals reproduce the experiment with satisfying (M06-L) to excellent (MN12-L) accuracy. This is also the case for B97-D3BJ. PBE0-D3 and BP86-D3 show again a great discrepancy from the experiment. B3LYP-D3 overestimates the ES slightly, but is still in a satisfying agreement, while the B3LYP functional shows a surprisingly good agreement with the experimentally derived activation barrier. For the solvent phase, all functionals predict, if compared directly, the hydrogenation of **4a** to be slower with **2** as precatalyst than with **1**. This is in line with the experimental results (17.2 ± 1.0 kcal/mol for precatalyst **1** compared to 21.1 ± 2.3 kcal/mol for precatalyst **2**).

4. DFT-Based Prediction of the Catalytic Cycle with 1 for the Hydrogenation of *trans*-Stilbene and Comparison with Experimentally Derived Energy Spans. In the previous sections, three different homogeneously catalyzed hydrogenations were investigated. Figure 14 shows the mean absolute deviation of the tested DFs from the experimentally determined activation barriers over the three hydrogenation reactions.

With regard to computational cost, Figure 15 summarizes the performance of four different DFs which perform well in terms of quantitative prediction of the ES. When the results shown in Figures 14 and 15 are evaluated together, it emerges very clearly that MN12-L as well as B97-D3BJ and B3LYP-D3 reproduce the experimentally obtained ESs with a pleasingly low deviation in the range of only 1 kcal/mol. This is one of the central results of this work: Modern dispersion corrected DFs are capable to predict ESs and other thermodynamic activation parameters in homogeneously catalyzed hydrogenations with an acceptably low deviation from experiment and in acceptable time frames!

The best compromise between accuracy and cost is B97-D3BJ, followed by MN12-L. M06-L shows a tendency to underestimate ESs in the 1−3 kcal/mol range, which still is a good result. B3LYP-D3 and CAM-B3LYP and all other DFs tested can be ruled out due to much higher computational cost or poor agreement with the experimental span.

These results show that the question if a computationally designed catalyst would be an active or an inactive catalyst for the hydrogenation of an olefin in a given temperature regime can clearly be answered by DFT computations in a reasonable time frame, when either B97-D3BJ or one of the Minnesota functionals is chosen. Accordingly, one would come to the conclusion that DFT can indeed be used as a catalyst design tool prior to experimental work in the field of catalytic hydrogenations.

To verify the conclusions made above, we chose *trans*-stilbene (**6**, Figure 16) and predicted computationally the activation barrier for the hydrogenation of this substrate with precatalyst **1**.

Due to the good quality of the computed ESs and the short calculation times, we used the MN12-L, B97-D3BJ, and the

DOI: 10.1021/jacs.5b11997
J. Am. Chem. Soc. XXXX, XXX, XXX−XXX

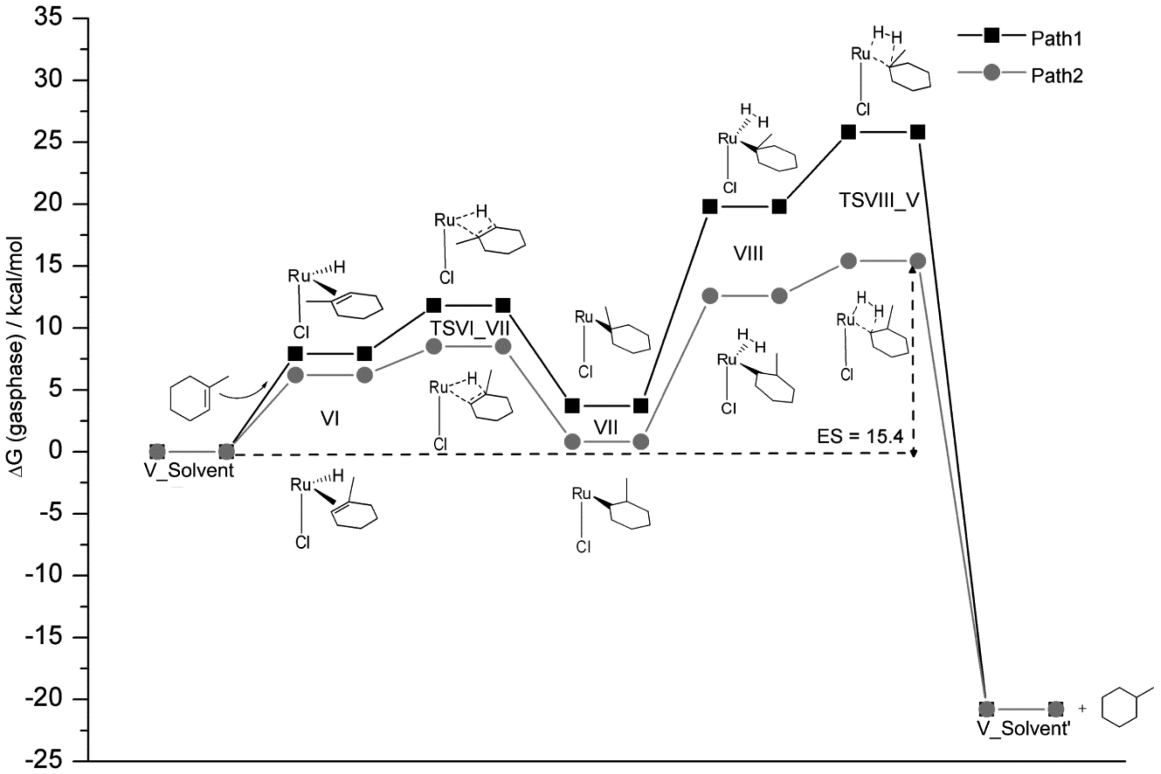

Figure 10. Gibbs free energy profile for the two possible hydrogenation pathways of 1-methylcyclohexene (**4b**) with precatalyst **1**.

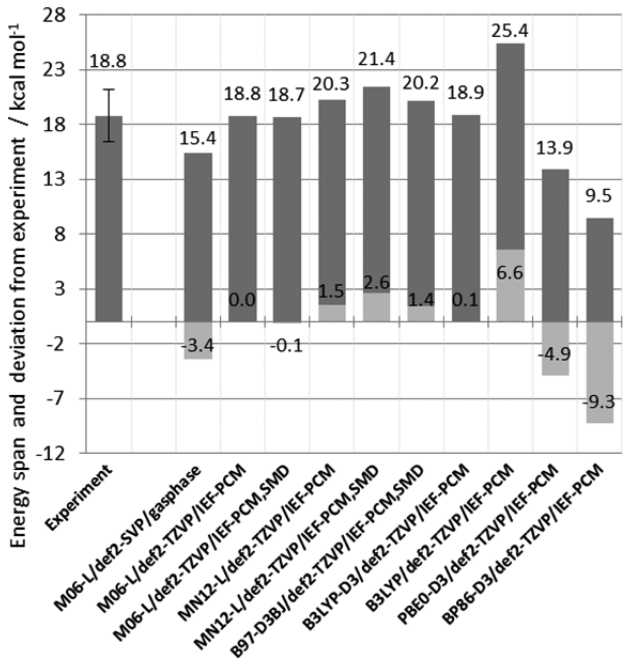

Figure 11. Experimental and computational energy spans (dark gray) and deviations from experiment (light gray) for the hydrogenation of **4b** with **1** as precatalyst. Solvent model calculations were performed with THF as solvent (see SI for details).

M06-L functionals with the def2-TZVP basis set and the IEF-PCM or SMD model for implicit solvent correction. Complete catalytic cycles for the hydrogenation of **6** were computed. The computed ESs range between 22.1 and 26.1 kcal/mol. These results suggest that the reaction will be possible and proceed with practical rates at slightly elevated temperatures around 50 °C. We subsequently performed the reaction at two different temperatures (40 and 60 °C), to verify the DFT-made predictions. It should be pointed out that experimentally the determination of the ES for the *trans*-stilbene hydrogenation consists of only two single experiments rather than on an Eyring plot. As predicted the reaction is possible, and **6** is converted fully to the hydrogenated product at 60 °C within 16 h reaction time. The results obtained are shown in Figure 17 together with the results obtained for cyclohexene and 1-methylcyclohexene hydrogenation with precatalyst **1**.

It can be seen convincingly also for the hydrogenation of **6** that the deviation between theory and experiment is small and in the expected range. Also the prediction pattern for the various DFs follows the trends, which were observed already for substrates **4a** and **4b**, indicating B97-D3BJ to be closest to the experimental value, while MN12-L tends to overestimate the ES slightly, and M06-L(IEF-PCM) underestimates the ES moderately.

When instead the two precatalysts **1** and **2** are compared the same results evolve: In Figure 18, the performance of the two complexes in the hydrogenation of **4a** is compared. The same trends are observed as for the above-mentioned comparison of different substrates. This indicates that DFT does also reproduce the relatively small differences in the catalyst activity generated by a different ligand very well. All these results clearly evidence that contemporary DFT is indeed a powerful tool to predict the ESs of catalytic cycles for olefin hydrogenations with an accuracy high enough to supply experimentalists with valuable information if the—presumably tedious and lengthy—synthesis of an unknown catalyst can be expected to be worthwhile with regard to the catalyst performance.

DOI: 10.1021/jacs.5b11997
J. Am. Chem. Soc. XXXX, XXX, XXX−XXX

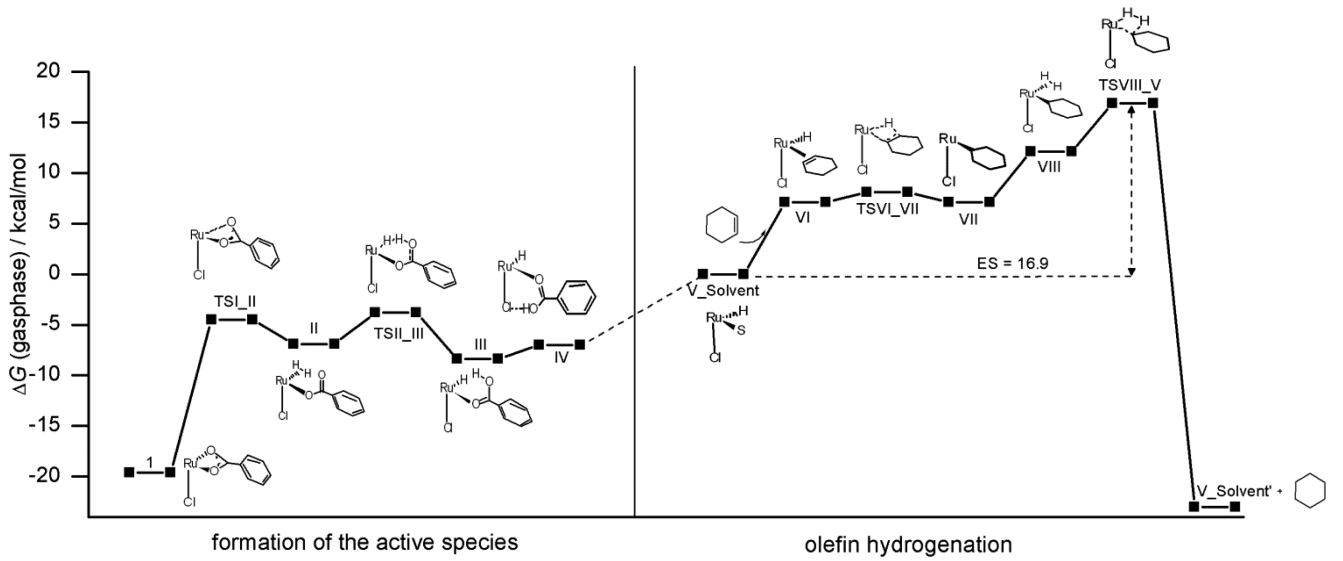

Figure 12. Gibbs free energy profile for the hydrogenation of cyclohexene (**4a**) with precatalyst **2**.

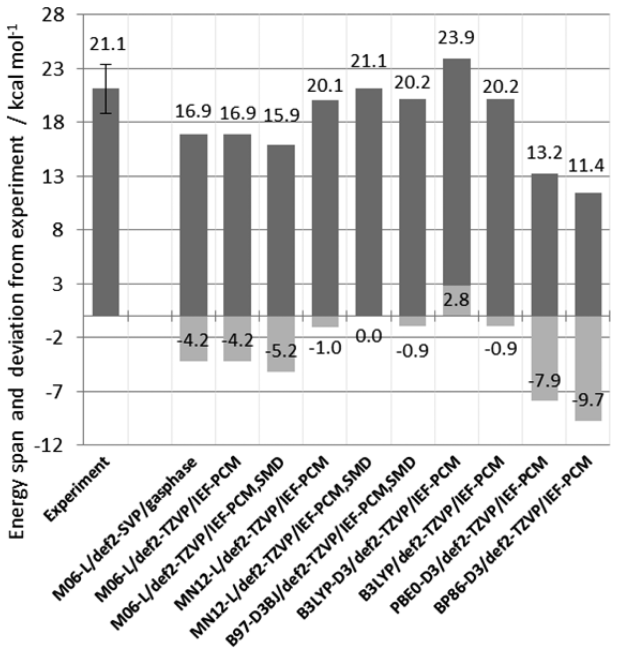

Figure 13. Experimental and computational energy spans (dark gray) and deviations from experiment (light gray) for the hydrogenation of **4a** with **2** as precatalyst. Solvent model calculations were performed with THF as solvent (see SI for details).

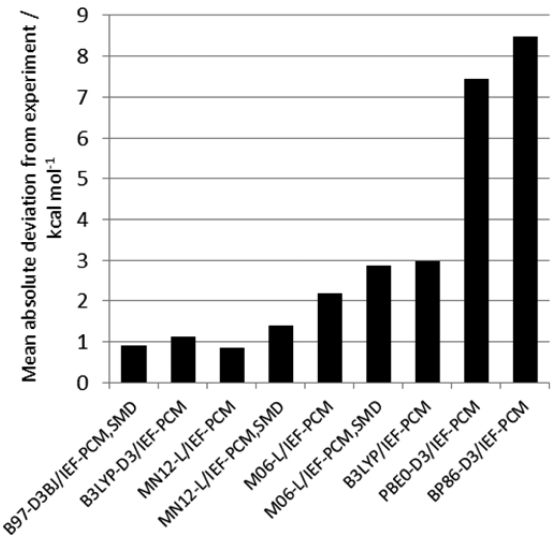

Figure 14. Mean absolute deviation of the ES in the three investigated cases of the tested DFs from the experiment. All calculations were performed with def2-TZVP basis set.

CONCLUSION

In this work the hydrogenation of cyclohexene (**4a**) with precatalysts **1** and **2**, and the hydrogenation of 1-methylcyclohexene (**4b**) with **1**, were investigated experimentally and by means of DFT computations. The aim of this work was to compare experimental and computed energy spans and answer the question if the experimental barriers can be reproduced by contemporary DFT calculations well enough to make DFT useful for predictive computational chemistry prior to exerpimental work. This was validated for the hydrogenation of *trans*-stilbene (**6**) with **1**.

Among the tested DFs the B97-D3BJ functional was very accurate in reproducing/predicting energy spans with deviations in the 1 kcal/mol range. Furthermore, in terms of computational cost it has evolved as the best-performing DF. The Minnesota functionals MN12-L and M06-L also lead to very accurate results in various cases. Also the computational cost is only marginally higher than that for B97-D3BJ. B3LYP-D3 is an accurate method to calculate energy spans, but has the drawback of significantly longer calculation times. All other DFs tested either show poor agreement with the experimental span or suffer from an inacceptably high computational cost. Accordingly, when B97-D3BJ, MN12-L, or M06-L is chosen, it can be concluded that contemporary DFT is capable of generating meaningful results which describe an energy landscape in catalytic olefin hydrogenation accurately enough to deduce decisions for experimental chemistry.

While more case studies covering other chemical transformations need to be carried out to check on the transferability of the results obtained in this case study for the DFs mentioned the following can be tentatively stated: If a plausible reaction mechanism can be proposed for an unknown catalyst in a

DOI: 10.1021/jacs.5b11997
J. Am. Chem. Soc. XXXX, XXX, XXX−XXX

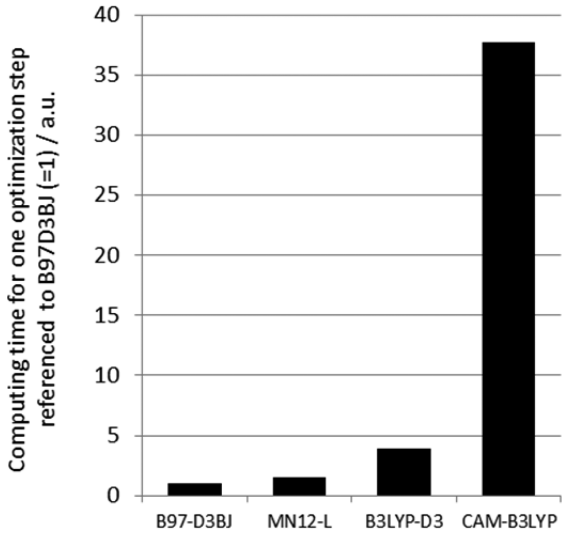

Figure 15. Average computing time for one optimization step on def2-TZVP level referenced to B97-D3BJ (=1).

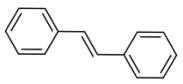

6

Figure 16. *trans*-Stilbene (**6**) as a model substrate for the prediction of activation barriers with DFT methods.

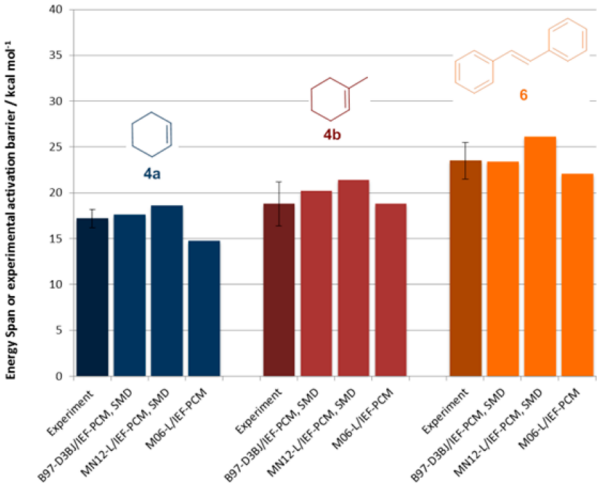

Figure 17. Comparison of experimental and computed energy spans derived for precatalyst **1** with different substrates.

desired transformation, the computation of energy spans by DFT methods is accurately enough and fast enough to provide a reliable check of the feasibility of such a catalytic cycle. In principle this can be applied as a screening tool to already known reactions as well as an exploration method for new transformations. This of course does not absolve somebody from checking carefully all imaginable side reactions to avoid to overlook stable minima contributing unfavorably to the energy span which might be reached via low lying transition states. Similarly, obvious catalyst deactivation processes should also be considered. There will always be subtleties to consider for each catalyst system under inspection, and difficult cases will always remain.[14,15] Accordingly, there is certainly no automated and

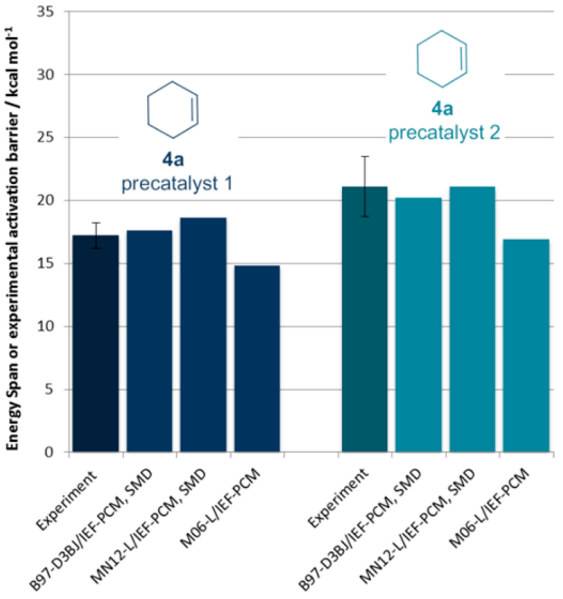

Figure 18. Comparison of experimental and computed energy spans derived for precatalyst **1** (left set of columns) and **2** (right set of columns) for substrate **4a**.

generally applicable catalyst structure search in sight which operates on a pressing-a-button basis. But from the results presented in this work it evolves that designing novel molecular catalysts can certainly be strongly supported by computational chemistry even *a priori* to experimental work.

■ ASSOCIATED CONTENT

Supporting Information

The Supporting Information is available free of charge on the ACS Publications website at DOI: 10.1021/jacs.5b11997.

Experimental procedures, analytical data for synthesis and characterization of the metal complexes, procedures of the catalytic experiments, computational details, and Cartesian coordinates of the stationary points (PDF)

X-ray crystallographic data for **1** and **2** (CIF)

■ AUTHOR INFORMATION

Corresponding Authors

*hoelscher@itmc.rwth-aachen.de

*leitner@itmc.rwth-aachen.de

Author Contributions

§K.R. and M.H. contributed equally.

Notes

The authors declare no competing financial interest.

■ ACKNOWLEDGMENTS

This work has been carried out as part of the International Research Training Group "Selectivity in chemo- and bio-catalysis" IRTG1628 (Seleca), which is funded by the german research foundation. This work was supported by the Cluster of Excellence "Tailor-Made Fuels from Biomass" (TMFB) which is funded by the Excellence Initiative of the German Federal and State Governments to promote science and research at German universities.

DOI: 10.1021/jacs.5b11997
J. Am. Chem. Soc. XXXX, XXX, XXX−XXX

REFERENCES

(1) (a) Jover, J.; Fey, N. *Chem. - Asian J.* **2014**, *9*, 1714−1723. (b) Tsang, A. S. K.; Sanhueza, I. A.; Schoenebeck, F. *Chem. - Eur. J.* **2014**, *20*, 16432−16441.

(2) (a) Cramer, C. J.; Truhlar, D. G. *Phys. Chem. Chem. Phys.* **2009**, *11*, 10757−10816. (b) Klippenstein, S. J.; Pande, V. S.; Truhlar, D. G. *J. Am. Chem. Soc.* **2014**, *136*, 528−546. (c) Sameera, W. M. C.; Maseras, F. *Wiley Interdisciplinary Reviews: Computational Molecular Science* **2012**, *2*, 375−385.

(3) (a) Goerigk, L.; Grimme, S. *Phys. Chem. Chem. Phys.* **2011**, *13*, 6670−6688. (b) Goerigk, L.; Kruse, H.; Grimme, S. *ChemPhysChem* **2011**, *12*, 3421−3433.

(4) (a) Peverati, R.; Truhlar, D. G. *Philos. Trans. R. Soc., A* **2014**, *372*, 20120476−20120476. (b) Zhao, Y.; Truhlar, D. G. *J. Chem. Phys.* **2006**, *125*, 194101. (c) Peverati, R.; Truhlar, D. G. *Phys. Chem. Chem. Phys.* **2012**, *14*, 13171−13174.

(5) (a) Weymuth, T.; Couzijn, E. P. A.; Chen, P.; Reiher, M. *J. Chem. Theory Comput.* **2014**, *10*, 3092−3103. (b) Jacobsen, H.; Cavallo, L. *ChemPhysChem* **2012**, *13*, 562−569. (c) McMullin, C. L.; Fey, N.; Harvey, J. N. *Dalton Trans.* **2014**, *43*, 13545−13556. (d) Ahlquist, M. S. G.; Norrby, P.-O. *Angew. Chem., Int. Ed.* **2011**, *50*, 11794−11797. (e) Nilsson Lill, S. O.; Ryberg, P.; Rein, T.; Bennström, E.; Norrby, P.-O. *Chem. - Eur. J.* **2012**, *18*, 1640−1649. (f) Gansäuer, A.; Seddiqzai, M.; Dahmen, T.; Sure, R.; Grimme, S. *Beilstein J. Org. Chem.* **2013**, *9*, 1620−1629. (g) Averkiev, B. B.; Truhlar, D. G. *Catal. Sci. Technol.* **2011**, *1*, 1526−1529. (h) McMullin, C. L.; Jover, J.; Harvey, J. N.; Fey, N. *Dalton Trans.* **2010**, *39*, 10833−10836. (i) Engle, K. M.; Lu, G.; Luo, S.-X.; Henling, L. M.; Takase, M. K.; Liu, P.; Houk, K.; Grubbs, R. H. *J. Am. Chem. Soc.* **2015**, *137*, 5782−5792.

(6) (a) Benitez, D.; Tkatchouk, E.; Goddard, W. A. *Organometallics* **2009**, *28*, 2643−2645. (b) Benitez, D.; Tkatchouk, E.; Goddard III, W. A. *Chem. Commun.* **2008**, 6194−6196.

(7) (a) Zhao, Y.; Truhlar, D. G. *Org. Lett.* **2007**, *9*, 1967−1970. (b) Yang, H.-C.; Huang, Y.-C.; Lan, Y.-K.; Luh, T.-Y.; Zhao, Y.; Truhlar, D. G. *Organometallics* **2011**, *30*, 4196−4200.

(8) (a) Lyngvi, E.; Sanhueza, I. A.; Schoenebeck, F. *Organometallics* **2015**, *34*, 805−812. (b) Kalvet, I.; Bonney, K. J.; Schoenebeck, F. *J. Org. Chem.* **2014**, *79*, 12041−12046.

(9) Gusev, D. G. *Organometallics* **2013**, *32*, 4239−4243.

(10) (a) Truscott, B. J.; Kruger, H.; Webb, P. B.; Bühl, M.; Nolan, S. P. *Chem. - Eur. J.* **2015**, *21*, 6930−6935. (b) Fernández-Alvarez, F. J.; Iglesias, M.; Oro, L. A.; Polo, V. *ChemCatChem* **2013**, *5*, 3481−3494. (c) Sieffert, N.; Réocreux, R.; Lorusso, P.; Cole-Hamilton, D. J.; Bühl, M. *Chem. - Eur. J.* **2014**, *20*, 4141−4155. (d) Grayson, M. N.; Krische, M. J.; Houk, K. *J. Am. Chem. Soc.* **2015**, *137*, 8838−8850.

(11) (a) Kozuch, S.; Shaik, S. *J. Am. Chem. Soc.* **2006**, *128*, 3355−3365. (b) Kozuch, S.; Shaik, S. *J. Phys. Chem. A* **2008**, *112*, 6032−6041. (c) Kozuch, S.; Shaik, S. *Acc. Chem. Res.* **2011**, *44*, 101−110.

(12) Kitamura, M.; Tokunaga, M.; Noyori, R. *J. Org. Chem.* **1992**, *57*, 4053−4054.

(13) Frisch, M. J.; Trucks, G. W.; Schlegel, H. B.; Scuseria, G. E.; Robb, M. A.; Cheeseman, J. R.; Scalmani, G.; Barone, V.; Mennucci, B.; Petersson, G. A.; Nakatsuji, H.; Caricato, M.; Li, X.; Hratchian, H. P.; Izmaylov, A. F.; Bloino, J.; Zheng, G.; Sonnenberg, J. L.; Hada, M.; Ehara, M.; Toyota, K.; Fukuda, R.; Hasegawa, J.; Ishida, M.; Nakajima, T.; Honda, Y.; Kitao, O.; Nakai, H.; Vreven, T.; Montgomery, J. A., Jr.; Peralta, J. E.; Ogliaro, F.; Bearpark, M. J.; Heyd, J.; Brothers, E. N.; Kudin, K. N.; Staroverov, V. N.; Kobayashi, R.; Normand, J.; Raghavachari, K.; Rendell, A. P.; Burant, J. C.; Iyengar, S. S.; Tomasi, J.; Cossi, M.; Rega, N.; Millam, N. J.; Klene, M.; Knox, J. E.; Cross, J. B.; Bakken, V.; Adamo, C.; Jaramillo, J.; Gomperts, R.; Stratmann, R. E.; Yazyev, O.; Austin, A. J.; Cammi, R.; Pomelli, C.; Ochterski, J. W.; Martin, R. L.; Morokuma, K.; Zakrzewski, V. G.; Voth, G. A.; Salvador, P.; Dannenberg, J. J.; Dapprich, S.; Daniels, A. D.; Farkas, Ö.; Foresman, J. B.; Ortiz, J. V.; Cioslowski, J.; Fox, D. J. *Gaussian09*, Revision D.01; Gaussian, Inc.: Wallingford, CT, 2009.

(14) Plata, R. E.; Singleton, D. A. *J. Am. Chem. Soc.* **2015**, *137*, 3811−3826.

(15) Winter, A. *Nat. Chem.* **2015**, *7*, 473−475.

DOI: 10.1021/jacs.5b11997
J. Am. Chem. Soc. XXXX, XXX, XXX−XXX